

## Preparation and Properties of Luminescent Lanthanide Based Graphene Oxide

Amanda L Jenkins<sup>1\*</sup>, David P Ziegler<sup>2</sup>, Erik Emmons<sup>3</sup> and Christopher J Karwacki<sup>4</sup>

<sup>1</sup>ASK Incorporated, 7447 Rockawalkin Road, Hebron, Maryland, 21830, USA

<sup>2</sup>US Army Natick RDE Center, Natick, Massachusetts, 01760, USA

<sup>3</sup>Science Applications International Corporation, 3465 Box Hill Corporate Center Drive, Abingdon, Maryland, 21009, USA

<sup>4</sup>Eggedwood Chemical Biological Center, 5183 Blackhawk Road, Gunpowder, Maryland, 21010, USA

### Abstract

Novel photoluminescent materials were prepared from the reaction of graphene oxide and luminescent lanthanides (europium, terbium, gadolinium, samarium, and dysprosium) in methanol at high pH. The binding of the lanthanides to graphene oxide through the oxygen functionality was evidenced by the sharp enhancement of laser induced luminescence and the appearance of peaks in specific regions of the spectra of the lanthanides. Raman spectroscopy indicated that the graphene oxide maintained its structure within the material and verified the complexation with the lanthanide. Surface morphology studies using SEM and TEM demonstrated the coverage of the graphene oxide surface by the lanthanide. Although some limited work has been published on europium and graphene oxide, this is the first study encompassing the majority of the luminescent lanthanides, taking full advantage of their capabilities including advanced electronic structure, raman and visible luminescence in a variety of colors.

**Keywords:** Lanthanides; Graphene; Luminescence; Raman; Europium; Terbium; Samarium; Gadolinium; Dysprosium

### Introduction

The use of lanthanides as probe ions and signal transducers in sensing applications is widely accepted, as they can often provide sensitivity in the parts per trillion range and lower [1]. Lanthanides comprise the largest naturally occurring group in the periodic table, and their similarities arise from a resemblance in the electronic configurations of the elements which consists of the xenon levels, filled 6s sublevel, and a varying amount of electrons occupying the 4f sublevel. Generally, the optical absorption and emission spectra of the ions formed by the triply charged free lanthanide ions consist of very narrow lines (0.1 nm-0.01 nm). Quantum mechanical calculations have indicated that the energies and the radial extensions of the 4f eigenfunctions dramatically drop at the beginning of the lanthanide series so that the maxima of the 4f eigenfunctions no longer exceed those of the 5s and 5p eigenfunctions [2]. Thus, the 4f orbitals are not the outermost shell, but are largely shielded from the external environment by the filled 5s and 5p shells. Since these 4f orbitals are shielded, the electrostatic field in lanthanide complexes, induced by coordinating ligands causes only small perturbations in the 4f electrons energy levels. As a result, the lanthanides within the complex retain their semi "atomic" nature which gives the characteristic narrow bands observed in lanthanide emission and excitation spectra [3,4].

These narrow features often result in analyses which are both selective and sensitive. The spectral position and intensity of these features are dependent on the environmental symmetry of the lanthanide complex [5]. As a result of this unique chemistry, lanthanides have been used for a variety of purposes such as catalysts, optical components, alternatives to radioisotopes, and as scientific probes for a wide variety of phenomena including probes of temperature [6,7] and structure (both electronic and crystalline) [8,9]. Trace analysis techniques based on lanthanide spectroscopy have also found application for detection of many compounds often at parts per trillion (ppt) levels or lower [10-12].

Europium is the most commonly used lanthanide for sensing applications for several reasons. First, the spectral splitting patterns

of europium are generally less complex (fewer peaks) and easier to interpret than the other lanthanides. Additionally, europium has the  $^5D_0 \rightarrow ^7F_2$  transition which is a "hypersensitive transition" reflecting even minor changes in its environment with very intense luminescence [13] (In this case the term luminescence is preferred over other terms such as fluorescence or phosphorescence because the intra-configurational transitions may or may not involve a change in spin) [5]. Europium is also the most reactive of the lanthanides because unlike most lanthanides which are primarily trivalent, europium also exists in the +2 state (electron configuration  $4f^7$ ) and the half-filled *f*-shell gives more stability [14].

Complexation by organic ligands was found to significantly enhance the luminescence intensity of the tripositive lanthanide, Ln(III) ions [1,14-17]. This enhancement was explained by a ligand to metal energy transfer mechanism [18,19]. The proposed mechanism indicates that when an excited triplet state of a coordinating ligand overlaps an excited lanthanide electronic level, the lanthanide luminescence is effectively pumped by the large cross section molecular absorbance of the ligand, rather than by the weak lanthanide absorbance. This process is believed to be much more efficient than direct absorption of light by the lanthanide since the lanthanides themselves exhibit low molar absorptivities. Proper ligand choice is therefore crucial in the preparation of lanthanide complexes.

Graphene oxide was selected as a coordinating ligand for the lanthanides because of its unique structural, electronic and optical properties [20], as well as its high mechanical strength [21]. The

**\*Corresponding author:** Amanda L Jenkins, ASK Incorporated, 7447 Rockawalkin Road, Hebron, Maryland, 21830, USA, Tel: 410-436-8660; E-mail: [Amanda21801@yahoo.com](mailto:Amanda21801@yahoo.com)

**Received** June 24, 2013; **Accepted** July 18, 2013; **Published** July 25, 2013

**Citation:** Jenkins AL, Ziegler DP, Emmons E, Karwacki CJ (2013) Preparation and Properties of Luminescent Lanthanide Based Graphene Oxide. J Phys Chem Biophys 3: 120. doi:10.4172/2161-0398.1000120

**Copyright:** © 2013 Jenkins AL, et al. This is an open-access article distributed under the terms of the Creative Commons Attribution License, which permits unrestricted use, distribution, and reproduction in any medium, provided the original author and source are credited.

complexation with graphene oxide would allow the lanthanide to be incorporated into a wide range of materials including field emission displays [22-24], sensors [25-27], thin film transistors [28-30], touch panels [31], electrodes for optoelectronic devices [32,33], fuel cells [34-36], solar cells [37,38], and batteries [39,40]. Graphene oxide was chosen over graphene because the intrinsic oxygen was needed to coordinate with the lanthanide. Limited studies have addressed the luminescence properties of graphene and graphene oxide [31]. However, the success has been limited by a lack of uniformity in treatment techniques and the inability to make materials that are strongly luminescent. The ability of graphene to quench the luminescence of fluorescent dyes has also been reported [41,42]. Lanthanides, on the other hand, have unique and strong luminescence properties. Combining the luminescence properties of lanthanides with the structural properties of graphene oxide was a natural step towards the creation of luminescent graphene materials.

In this study, europium, terbium, gadolinium, samarium or dysprosium were selected as potential candidates, since they have partially filled subshells which provide them with enhanced sensitivity to the environment and increased luminescence properties. Since each lanthanide has luminescence in a different region of the spectra, incorporating several provided graphene oxide materials that luminesced in many colors. The resulting europium, terbium, samarium, dysprosium, and gadolinium complexes with graphene oxide (GO), were verified by raman, and laser induced luminescence. The surface morphology and physical properties of the graphene/lanthanide materials (europium and terbium) were investigated by SEM and TEM.

## Experimental

### Reagents

Unless otherwise indicated, materials were obtained from commercial suppliers and used without further purification. Analytical reagent grade chemicals were used along with deionized water to prepare solutions. The lanthanides were obtained from Aldrich (Aldrich, Milwaukee, WI). The graphene oxide was prepared by Teresa Bandosz at the City College of New York (CUNY) and used as received [43].  $\text{Eu}(\text{NO}_3)_3 \cdot 5\text{H}_2\text{O}$  was prepared by taking  $\text{Eu}_2\text{O}_3$  and dissolving it in water with heat and just enough nitric acid to produce a clear solution. The resulting solution was evaporated to near dryness, and then left to crystallize. The resulting solid was evaluated spectroscopically to confirm the conversion. The remaining lanthanides were purchased as nitrates and used as obtained.

### Instrumentation

Luminescence was measured using a model 35-LAP-321-120 argon ion laser for excitation (Melles Griot, Carlsbad, CA). Holographic filters at 488 nm and 514 nm (Kaiser Optical Systems, Ann Arbor, MI, USA) were used to exclude all other laser lines. Spectra were collected using an  $f/4$ , 0.5-m monochromator (Chromex, Albuquerque, NM) equipped with a model ST-6 CCD (Santa Barbara Instruments Group, Santa Barbara, CA) using Kestrel Spec Software (K&M Co., Torrance, CA). Spectra were also obtained with a StellarNet Blue wave miniature fiber optic spectrometer (StellarNet, Tampa, FL) with a range 500-700 nm equipped with a 2400 g/mm ruled grating, a 2048 element detector array, integrated order sorting filter, 16-bit digitizer, and a 25  $\mu\text{m}$  slit and running SpectraWiz software. The excitation and emission light was carried to and from the sample using a 400  $\mu\text{m}$  bifurcated multimode fiber (Thor Labs, Newton, NJ). Scanning electron micrographs were

obtained using a JEOL 6300F Field Emission Scanning Electron Microscope SEM (JEOL, Ltd., Tokyo).

Transmission Electron Micrographs were obtained by placing small amount of powder into a vial of Methanol and ultrasonicated them using a Branson B-12 80 watt ultrasonic cleaner for 5 minutes. Once the particles were suspended, a small amount of liquid was drawn off using a pipette and placed drop-wise onto a holey carbon film copper TEM grid purchased through SPI Supplies and allowed to air dry on clean filter paper. Prior to use, the holey carbon film TEM grids were pre-cleaned with de-ionized water to remove as much adsorbed silicon and other detritus from SPI Supplies manufacturing process. The particle samples were then imaged using a JEOL FasTEM 2010 TEM at 200 kv using a Gatan Corp. Gatan Image Filter (GIF 2000) digital camera and the Energy Dispersive X-ray Spectrometry was recorded using an EDAX Corp. Genesis Si(Li) 30 mm<sup>2</sup> EDS detector system with the TEM operated in S (TEM) mode.

Raman samples were analyzed on an aluminum substrate using a Jasco NRS-3000 (Jasco Inc. Easton, MD) at 229 nm, 532 nm, and 785 nm. Samples were analyzed using a 2400 groove/mm grating with slits set to 100 microns and integration times between 20-30 seconds depending on the sample.

### Compound preparation

Graphene oxide was prepared by Teresa Bandosz, (City College New York) and used as obtained. Graphene oxide/europium materials were first prepared following the procedure outlined by Kim et al. [44]. The graphene oxide (0.5 g), water (20 mL) and NaOH (1 M aqueous solution, 1 mL) were sonicated for 30 minutes in a Cole-Parmer sonicator at 200 W. Europium nitrate,  $\text{Eu}(\text{NO}_3)_3 \cdot 5\text{H}_2\text{O}$  (0.428 g, 1 mmol) was added and stirred overnight. The solids were centrifuged, washed with water and acetone. The graphene/europium (Eu(GO)) solids were air dried on a watch glass overnight. This procedure was repeated with increasing amounts of europium nitrate (1.0 g, 1.25 g, 1.5 g and 2.0 g). The same procedure described above was repeated for terbium, gadolinium, samarium, and dysprosium nitrate.

### Compound evaluation

The graphene oxide, europium oxide, lanthanide nitrates and the resulting lanthanide graphene oxide samples were evaluated using the laser induced fluorescence system described above. Excitation wavelengths of 465.8 nm, 488 nm, 496 nm, and 514 nm were evaluated for all materials. Optimal wavelengths were selected for each material: 488nm for the europium, and samarium complexes, 254 nm for gadolinium and 514 nm selected for the terbium complexes. An optimal wavelength for dysprosium was not able to be determined using the excitation sources available.

The lanthanide graphene oxide compounds with the highest overall luminescence intensity, (europium and terbium graphene oxide) were selected for SEM and TEM.

## Results and Discussion

As expected, the europium samples exhibited the greatest intensity (visibly red/orange) and interpretation of its spectral line patterns was easiest (based on number of peaks). Europium benefits from being 1 electron short of a half full shell making it easy for it to accept the electron for strong energy transitions. The conversion from europium oxide to europium nitrate was confirmed spectroscopically by a comparison with the spectra published by Buenzli and Yersin [45]. Europium samples were evaluated using excitation wavelengths of

465.8 nm, 472.7 nm, 488.0 nm, and 514.5 nm. Excitation at 465.8 nm was determined to have the highest luminescence intensity and give the best peak resolution, confirming previously published results [5]. Complexation between the lanthanide and the graphene oxide was determined by spectral changes and increased luminescence when compared with the luminescence of the lanthanide and the graphene oxide by themselves (Figure 1). The europium graphene oxide sample with the highest luminescent intensity was that prepared with 1.5 g of europium nitrate. The sample prepared with 0.5 g showed no spectral difference from the graphene oxide sample. This trend of highest luminescence for the complexes prepared 1.5 g of lanthanide nitrate was followed for all the lanthanides examined in this study, and it was these samples that were chosen for full characterization.

In comparing the luminescence spectra of graphene oxide, europium nitrate and europium graphene oxide several transitions were evaluated. The  $^5D_0 \rightarrow ^7F_1$  transition of the europium (from about 590-595 nm) exhibited a 1 nm shift when converted from the nitrate complex at 592 nm and the Eu(GO) complex at 591 nm. Additionally, the two peaks in the 595 nm region are better resolved in the Eu(GO) complex. The Eu(GO) peak at 595 nm is also higher in intensity, however this could be due to the fact that the GO itself has a fluorescence peak at that wavelength.

The hypersensitive  $^5D_0 \rightarrow ^7F_2$  europium transition was also evaluated for evidence of Eu(GO) complex formation. The europium nitrate peak at 615 nm was shifted one nanometer to the blue (614 nm) in the Eu(GO) and also reduced in intensity relative to the peak at 617.5 nm. The peak at 617.5 nm was shifted 0.1 nm to the blue in the nitrate complex. Comparing these splitting patterns with the calculations done by Carlos et al. [15] (and taking into account no peaks were seen in the  $^5D_0 \rightarrow ^7F_1$  transition) the site symmetry for both molecules is likely  $D_2$  or  $D_2d$  with either a tetragonal or rhombic crystal system. If only one transition could be analyzed for binding, this would be the one chosen due to its sensitivity and intensity.

The terbium, samarium, gadolinium, and dysprosium samples were evaluated in a similar manner with the results summarized in Table 1. The terbium complexes (excited at 514 nm) exhibited the second strongest luminescence (visibly green) and had the next easiest spectra to evaluate (Figure 2). Terbium has higher intensity bands than expected because, like europium, it is one electron away from having a half full (stable) f shell. This makes promotion of the extra electron easier and gives rise to stronger luminescence. The first transition evaluated, the  $^5D_4 \rightarrow ^7F_5$  had the strongest luminescence. In this spectral region, three peaks were seen for the terbium nitrate (541.5 nm, 543.3 nm, and 545.8 nm) while only two peaks were noted for the Tb(GO) complex (544.5 nm and 547.0 nm). The intensity of the largest peak also red shifted from the nitrate to the Tb(GO). In the  $^5D_4 \rightarrow ^7F_4$  transition, the terbium nitrate has 2 unresolved peaks (581.0 nm and 585.25 nm) while the Tb(GO) complex has only one (585.0 nm). The  $^5D_4 \rightarrow ^7F_3$  transition has one peak at 621.5 nm for the nitrate and two unresolved peaks at 621.3 and 622.8 nm in the Tb(GO) complex. The GO and Tb(GO) complex both had weak peaks at 536.8 nm and 593.8 nm which were not seen in the terbium nitrate spectrum.

The gadolinium, situated on the periodic table between europium and terbium does not have the same intense luminescence characteristics as its neighbors because it has the stability of a half filled f shell making it very difficult to promote an electron to the excited state. An excitation wavelength of 488 nm was used for the gadolinium complexes. 488 nm is not necessarily the optimal excitation wavelength for gadolinium but it was the strongest band output by the laser available, and gave the best

results. UV excitation using a hand held type uv-light at 254 nm and 365 nm was also attempted with no success. As seen in the previous complexes the gadolinium graphene oxide had an overall luminescence increase over the nitrate and was much more intensely luminescent than the graphene oxide alone (Figure 3). New strong luminescence bands were seen in the 600 nm-620 nm region, as well as peak shifts and splitting changes in the 660 nm-670 nm, 740 nm-755 nm, and 785 nm-800 nm regions. These changes were attributed to the complexation of the gadolinium and the graphene oxide. There are so many bands associated with gadolinium complexes that assigning the transitions with certainty was not possible, and spectral changes were identified by region of the spectrum.

Samarium, the lanthanide immediately preceding europium has many absorption bands in the region below 500 nm and efficient fluorescence occurs from the  $^4G_{5/2}$  level for solid materials. The emission

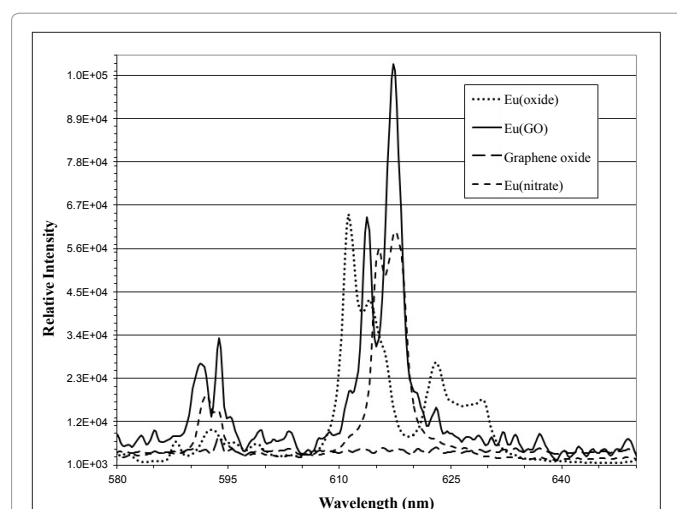


Figure 1: Spectra of the europium, graphene oxide, and the Eu(GO) showing the changes that occur with co-ordination. The europium and graphene oxide are shown on the right axis for better comparison. Excitation wavelength 488 nm.

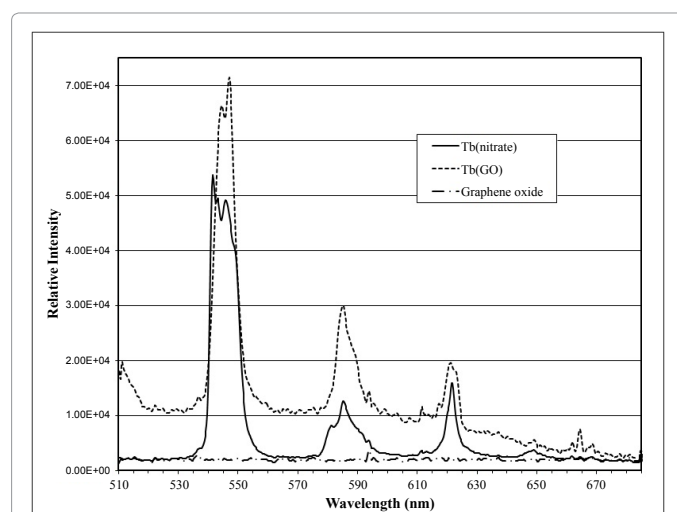


Figure 2: Spectra of the terbium, graphene oxide, and the Tb(GO) complex showing the changes that occur with co-ordination. The terbium nitrate and graphene oxides are shown on the right axis for better comparison. Excitation wavelength 514.0 nm.

is divided between many terminal levels making spectral interpretation difficult, and many ion-ion self quenching transitions are possible [13]. The preparation of the samarium complexes was also more difficult. The materials had to be purified by dissolving the materials in equal parts water/methanol and recrystallizing. Excited at 488 nm, the overall luminescence increase from the samarium nitrate to the samarium graphene oxide complex was not as intense as that seen for europium and terbium (Figure 4). Wavelengths of 254 nm, 465.8 nm, 472 nm, and 514 nm were also evaluated but gave no notable luminescence. As expected, the spectrum was much more complicated than that of terbium or europium making it less useful as a probe ion but still providing another color region for optical applications. Confirmation of complexation between the samarium and the graphene oxide was verified by spectral changes in several regions. In the transitions  ${}^4G_{5/2} \rightarrow {}^6H_{5/2}$  (580 nm-600 nm region),  ${}^4G_{5/2} \rightarrow {}^6H_{7/2}$  (600 nm-620 nm region), and  ${}^4G_{5/2} \rightarrow {}^6H_{9/2}$  (640 nm-660 nm region) peak splitting changes were noted as well as the appearance as new intense luminescence bands. In the  ${}^4G_{5/2} \rightarrow {}^6H_{11/2}$  transition (740 nm-770 nm region) splitting changes and peak shifts were noticed as well as an intensity increase. In the  ${}^4G_{5/2} \rightarrow {}^6F_{7/2}$  transition (790 nm-820 nm region) splitting changes and peak shifts were observed between the nitrate and samarium graphene oxide complex. All of these indicate successful coordination of the materials.

Dysprosium, the lanthanide immediately following terbium, was also reacted with graphene oxide and evaluated. Regardless of the excitation used, no changes were detected between the dysprosium nitrate and the dysprosium graphene oxide material. The synthesis was attempted many times using many different ratios with little luminescence response from any of them. The energy levels for dysprosium are typically very high making it hard to excite without complexation with organic ligands to provide intersystem crossing and it is surmised that the graphene oxide does not provide the levels needed. The raman spectra did exhibit significant changes between the nitrate and the graphene oxide complexes which supports this conclusion.

The SEM analysis was performed on the graphene oxide as well as the europium and terbium graphene oxide materials in an effort to better understand what was going on at the surface. The SEM of the graphene oxide showed the expected sheet like structure. In the europium graphene oxide as well as the terbium graphene oxide SEM images the sheet like structure can still be identified and the large lanthanide ions are seen to cover the surface (Figure 5).

TEM images were also collected for the europium and terbium graphene oxide particles (Figure 6). High resolution analysis of the europium graphene oxide particles shows limited graphene crystallinity. EDS data collected on the sample found the expected europium, oxygen, and carbon. The X-ray mapping illustrated the strong correlation of the europium being bound to the graphene oxide particles. The lower magnification TEM images for the terbium graphene oxide particles sample showed the graphene present as mostly planar flakes. The high magnification TEM indicated that the particles exhibited good crystallinity of the graphene as the atomic lattice features of the graphene particles were clearly visible. The EDS spectra confirmed the presence of terbium, oxygen, and carbon in the sample while X-ray mapping showed the uniform coverage of the terbium on the graphene oxide particles.

Raman analysis was performed on each of the lanthanide nitrates, the lanthanide graphene oxide materials and the graphene oxide itself. The raman was primarily used to verify the binding of the graphene oxide with the lanthanide. The raman spectra also confirmed the graphene oxide maintained its structure within the lanthanide based materials as indicated by the bands at  $1400\text{ cm}^{-1}$  (D band) and  $1600\text{ cm}^{-1}$  (G band) region of the spectra. The raman spectra of the terbium species are shown in Figure 7. In addition to the graphene oxide characteristics, the raman also indicated that there is still evidence of some residual nitrate co-ordinated within the materials.

## Conclusions

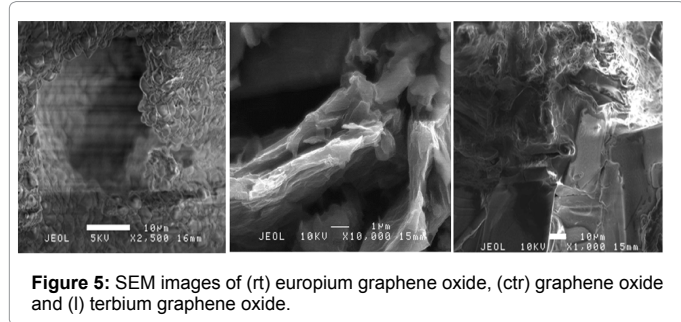
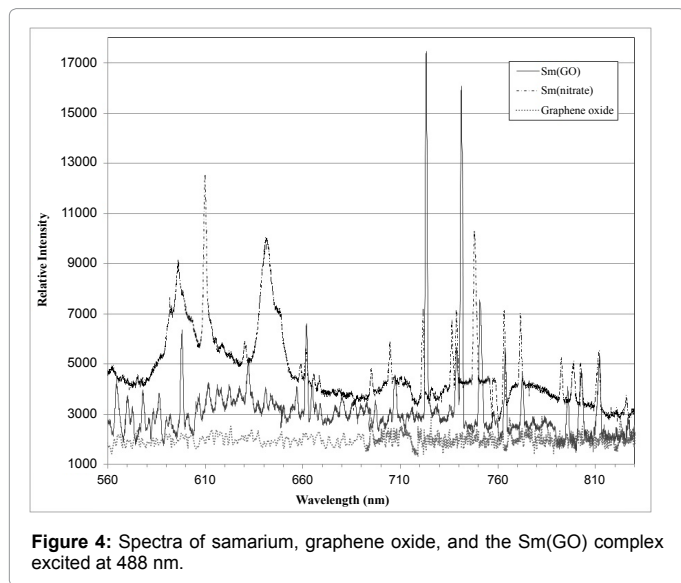
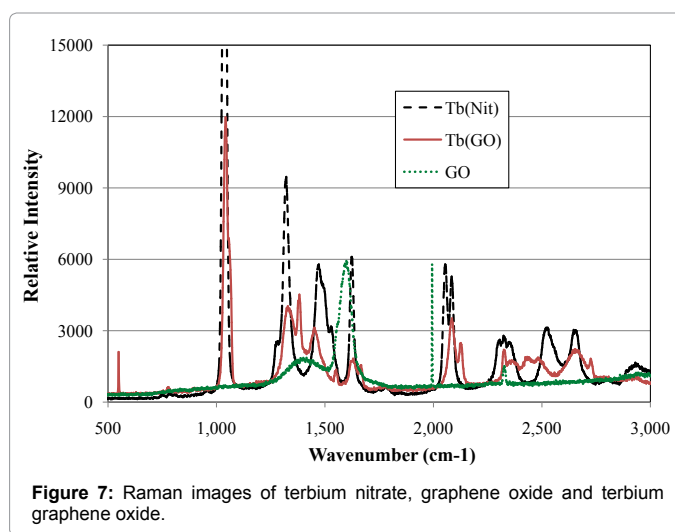
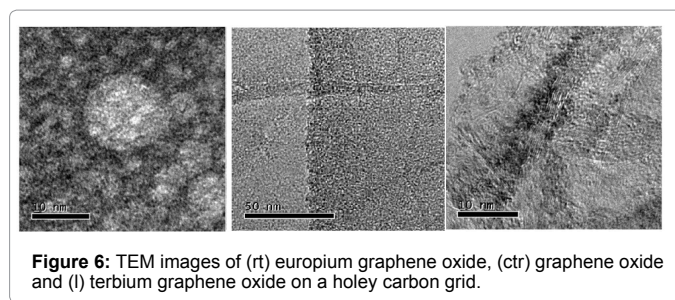
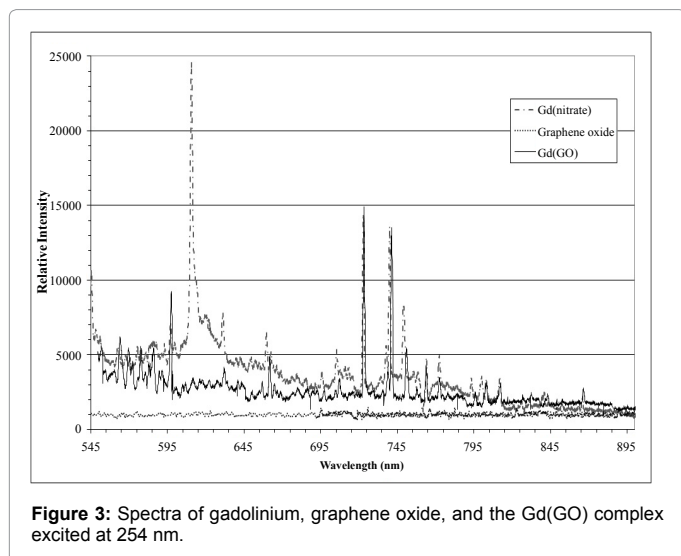
The ability to co-ordinate luminescent lanthanides with graphene

| Wavelength Region | Graphene oxide | Europium oxide                             | Europium nitrate       | Europium graphene oxide            | Terbium nitrate        | Terbium graphene oxide | Samarium nitrate  | Samarium graphene oxide   | Gadolinium nitrate  | Gadolinium graphene oxide                                     |
|-------------------|----------------|--|------------------------|------------------------------------|------------------------|------------------------|---|---|---|---|
| 500-550 nm        |                |  |                        |                                    | s 542 (h)<br>s 548 (l) | s 543 (l)<br>s 549 (h) |   |   |   |   |
| 551-600 nm        | s 595 (l)      | s 587 (l)<br>s 593(l)                      | d 590-595              | d/t 588-597                        | d 579-595              | d 580-594              | d 590-605   | s 600 (l)   | s 587 (l)   | s 597 (h)   |
| 601-650 nm        |                | s 610.5 (h)<br>s 614 (l)<br>s 623<br>s 630 | s 614 (h)<br>s 618 (h) | s 613 (l)<br>s 618 (h)<br>s 623(l) | s 623 (l)              | d 615-625              | s 614 (h)<br>d 640-655  | s 625 (l)   | s 615 (h)<br>s 620 (h)<br>s 631 (l)<br>s 635 (l)  | s 635 (l)   |
| 651-700 nm        |                |  |                        |                                    |                        |                        | s 695 (l)   | s 658 (l)<br>s 662 (l)<br>s 698 (l)   | d 662-665 (l)   | s 663.5 (h)   |
| 701-750 nm        |                |  |                        |                                    |                        |                        | s 707 (l)<br>s 711 (h)<br>s 740 (l)<br>s 745 (l)<br>s 750 (l) | s 709 (l)<br>s 713 (h)<br>s 738 (l)<br>s 740 (h)  | s 724 (h)<br>s 739 (l)<br>s 741 (h)   | s 706 (l)<br>s 724.5 (l)<br>s 741 (h)<br>s 742 (h)            |
| 750- nm           |                |  |                        |                                    |                        |                        | s 761 (l)<br>s 770 (l)<br>s 793 (l)<br>s 800 (l)<br>s 810 (l) | s 752 (l)<br>s 762 (l)<br>s 775 (l)<br>s 771 (l)<br>s 797 (l)<br>s 802 (l)<br>s 811 (l) | s 752 (l)<br>s 765 (l)<br>s 775 (l)<br>s 793 (l)<br>s 800 (l)<br>s 802 (l)<br>s 812 (l) | s 753 (l)<br>s 765 (l)<br>s 796 (l)<br>s 802 (l)<br>s 812 (l) |

(s) singelet peak(d) doublet peaks (t) triplet peaks (h) high intensity peak (l) low intensity peak

Table 1: Major peaks in Graphene Oxide/Lanthanide spectra.

oxide has been established, providing a new set of building blocks for future generations of nanomaterials. The combination of mechanical strength and electronic properties provide by the graphene oxide enhanced by the strong luminescence and magnetic properties of the lanthanides will provide materials for sensors and displays that can be incorporated into fabrics, battery materials and fuel cells with built in residual life indicators, and many other applications. The inclusion of



several lanthanides in this study will allow the materials to be much more tunable to color, and magnetism that provide a wider range of chemical applications that could expand the fields of supramolecular chemistry.

#### Acknowledgements

The authors would like to thank the Edgewood Chemical Biological Center (ECBC) and the Surface Science Initiative for financial support. Additionally we would like to thank Dr. Erica Valdes (ECBC) for SEM support and Dr. Alex Balboa (ECBC) and Dr. Greg Mogilevsky (Booz Allen Hamilton) for review and useful discussion.

#### References

- Jenkins AL and Murray GM (1996) The Ultratrace Determination of Lanthanides by Luminescence Enhancement. *Anal Chem* 68: 2974-2980.
- Stump NA (1991) A Study of Lanthanide Fluorescent Shifts Caused by Near Neighbor Perturbation. University of Tennessee, Knoxville.
- Cotton S (1991) Lanthanides and Actinides. Oxford University Press, New York.
- Murray GM, Pesterfield LL, Stump NA, Schweitzer GK (1989) Effects of Inorganic Counterions on the Fluorescence Spectra of the Tetrakis(1-phenyl-1,3-butanedionato)europium(III) Anion. *Inorg Chem* 28: 1994-1998.
- Jenkins AL (1998) Polymer Based Lanthanide Fluorometric Sensors for the Detection of Chemical Agents. University of Maryland, Baltimore County.
- Gualtieri DM, Emo SM, Kinney TR (1991) Bismuth-Rare-Earth-Iron Garnet Composition for a Magneto-Optical Wheel Rotation Rate Sensor. *Appl Phys* 69: 5978-5981.
- Klakamp SL, Horrocks WD (1992) Lanthanide ion luminescence as a probe of DNA structure. *J Inorg Biochem* 46:175-205.
- Bünzli JCG, Plancherel D, Pradervand GO (1989) The europium(III) ion as luminescent probe: structural investigation of complexes between europium nitrate and two polyethers. *J Phys Chem* 93: 980-984.

9. Thompson JW, Susetyo W, Carreira LA (1996) *Appl Spectroscopy* 50: 401-408.
10. Jenkins AL, Buettner LC, Ellzy MW (2012) Molecularly imprinted polymer sensors for detection in the gas, liquid, and vapor phase. *J Mol Recognit* 25: 330-335.
11. Hannien P, Harma H (2011) *Lanthanide Luminescence: Photophysical, Analytical and Biological Aspects*. Springer Publishers, New York.
12. Orcutt KM, Jones WS, McDonald A, Schrock D, Wallace KJ (2010) A Lanthanide-Based Chemosensor for Bioavailable Fe<sup>3+</sup> Using a Fluorescent Siderophore. *Sensors (Basel)* 10: 1326-1337.
13. Edelstein NM (1980) *Lanthanide and Actinide Chemistry and Spectroscopy*. American Chemical Society Publishers, Washington, DC 267-274.
14. Greenwood NN, Earnshaw A (1984) *Chemistry of the Elements*. (1stedn), Pergamon Press, Oxford 1423-1449.
15. Carlos LD, Ferreira RA, Bermudez Vde Z, Ribeiro SZ (2009) Lanthanide-Containing Light-Emitting Organic-Inorganic Hybrids: A Bet on the Future. *Adv Mater* 21: 509-534.
16. Bernardo PD, Melchior A, Tolazzi M, Zanonato PL (2012) Thermodynamics of lanthanide(III) complexation in non-aqueous solvents. *Coord Chem Rev* 256: 328-351.
17. Xu HB, Deng JG, Kang B (2013) Designed synthesis and photophysical properties of multifunctional hybrid lanthanide complexes. *RSC Adv* 3: 11367-11384.
18. Crosby GA, Kasha M (1958) Intramolecular energy transfer in ytterbium organic chelates. *Spectrochim Acta* 10: 377-381.
19. Crosby GA, Whan RA, Alire RM (1961) Luminescent properties of some ternary complexes of europium with thenoyltrifluoroacetone and organic bases. *J Chem Phys* 34: 743-750.
20. Novoselov KS, Geim AK, Morozov SV, Jiang D, Zhang Y, et al. (2004) Electric Field Effect in Atomically Thin Carbon Films. *Science* 306: 666-669.
21. Lee C, Wei XD, Kysar JW, Hone J (2008) Measurement of the Elastic Properties and Intrinsic Strength of Monolayer Graphene. *Science* 321: 385-388.
22. Tien H, Huang Y, Yang S, Wang J, Ma CM (2011) The production of graphene nanosheets decorated with silver nanoparticles for use in transparent, conductive films. *Carbon* 49: 1550-1560.
23. Vadukumpully S, Paul J, Valiyaveetil S (2009) Cationic surfactant mediated exfoliation of graphite into graphene flakes. *Carbon* 47: 3288-3294.
24. Yoon BJ, Hong EH, Jee SE, Yoon DM, Shim D S, et al. (2005) Fabrication of Flexible Carbon Nanotube Field Emitter Arrays by Direct Microwave Irradiation on Organic Polymer Substrate. *J Am Chem Soc* 127: 8234-8235.
25. Shao Y, Wang J, Wu H, Liu J, Aksay I, et al. (2010) Graphene Based Electrochemical Sensors and Biosensors: A Review. *Electroanalysis* 22: 1027-1036.
26. Liu Y, Dong X, Chen P (2012) Biological and chemical sensors based on graphene materials. *Chem Soc Rev* 41: 2283-2307.
27. Pumera M, Ambrosi A, Bonanni A, Chang ELK, Poh HL (2010) Graphene for electrochemical sensing and biosensing. *TrAC* 29: 954-965.
28. Sun Q, Kim JH, Park JH, Seo S (2010) Characteristics of a pentacene thin film transistor with periodic groove patterned poly(methylmethacrylate) dielectrics. *Appl Phys Lett* 96 3: 103301-103303.
29. Yan C, Cho J, Ahn J (2012) Graphene-based flexible and stretchable thin film transistors. *Nanoscale* 4: 4870-4882.
30. Lee SK, Jang HY, Jang S, Choi E, Hong B, et al. (2012) All Graphene-Based Thin Film Transistors on Flexible Plastic Substrates. *Nano Lett* 12: 3472-3476.
31. Plume A (2010) Buckyballs, nanotubes and graphene: On the hunt for the next big thing. *Research Trends* 5-7.
32. Hellstrom SL, Lee HW, Bao ZN (2009) Polymer-Assisted Direct Deposition of Uniform Carbon Nanotube Bundle Networks for High Performance Transparent Electrodes. *ACS Nano* 3: 1423-1430.
33. Gilje S, Han S, Wang M, Wang KL, Kaner RB (2007) A Chemical Route to Graphene for Device Applications. *Nano Lett* 7: 3394-3398.
34. Seger B, Kamat PV (2009) Electrocatalytically Active Graphene-Platinum Nanocomposites. Role of 2-D Carbon Support in PEM Fuel Cells. *J Phys Chem C* 113: 7990-7995.
35. Srivastava S, Jain K, Singh VN, Singh S, Vijayan N, et al. (2012) Faster response of NO<sub>2</sub> sensing in graphene-WO<sub>3</sub> nanocomposites. *Nanotechnology* 23: 205501.
36. Yoo E, Okata T, Akita T, Kohyama M, Nakamura J, et al. (2009) Enhanced electrocatalytic activity of Pt subnanoclusters on graphene nanosheet surface. *Nano Lett* 9: 2255-2259.
37. Wang X, Zhi LJ, Tsao N, Tomovic Z, Li JL, et al. (2008) Transparent carbon films as electrodes in organic solar cells. *Angew Chem Int Ed Engl* 47: 2990-2992.
38. Wu J, Becerril H, Bao Z, Liu Z, Chen Y, et al. (2008) Organic solar cells with solutionprocessed graphene transparent electrodes. *Appl Phys Lett* 92: 263302.
39. Yoo E, Kim J, Hosono E, Zhou H, Kudo T, et al. (2008) Large reversible Li storage of graphene nanosheet families for use in rechargeable lithium ion batteries. *Nano Lett* 8: 2277-2282.
40. Wang DH, Choi DW, Li J, Yang Z, Nie Z, et al. (2009) Self-Assembled TiO<sub>2</sub>-Graphene Hybrid Nanostructures for Enhanced Li-Ion Insertion. *ACS Nano* 3: 907-914.
41. Kim J, Cote LJ, Kim F, Huang J (2010) Graphene oxide sheets at interfaces. *J Am Chem Soc* 132: 8180-8186.
42. Dantham V, Bisht P, Kalanoor B, Baby T, Ramaprabhu S (2012) Restricting charge transfer in dye-graphene system. *Chem Phys Lett* 521: 130-133.
43. Seredych M, Bandosz T (2007) The mechanism of ammonia retention on graphite oxides: Role of surface chemistry and structure. *J Phys Chem* 111: 15596-15604.
44. Kim JY, Lee JB, Kim HJ, Shin K, Yu YS, et al. (2010) Preparation and Physical Properties of Red-photoluminescent Graphene/Europium(III)/Picolinate. *Bull Korean Chem Soc* 31: 1485-1488.
45. Buenzli JCG, Yersin JR (1979) Fluorescence spectra and lifetime measurements of aqueous solutions of europium nitrate and perchlorate. *Inorg Chem* 18: 605-607.